JOURNAL OF GEOPHYSICAL RESEARCH, VOL. 105, NO. D7, PAGES 9003–9023, APRIL 16, 2000

Simulations of water vapor in the lower stratosphere and upper troposphere

Andrew Gettelman[1] and James R. Holton
University of Washington, Seattle

Anne R. Douglass
NASA/Goddard Space Flight Center, Greenbelt, Maryland

Abstract. A three-dimensional Chemical Tracer Model is used to simulate the distribution of water vapor in the upper troposphere (UT) and lower stratosphere (LS). The simulations include only the large scale advection of water vapor and the restriction that the air be at or below saturation at all times. This simulation is used to help distinguish among those processes that control water vapor in the UT/LS. The exchange of water vapor across the tropopause is analyzed in detail. The simulation qualitatively reproduces the water vapor distribution given by satellite and radiosonde observations on both sides of the tropopause, confirming the importance of the global temperature distribution and advection in controlling the water vapor distribution. Quantitative differences with observations of water vapor are ascribed to input temperature biases. Water vapor enters the stratosphere at all longitudes in the tropics. Details of subgrid-scale dynamic and convective processes are not necessary to explain the entry of water vapor into the stratosphere, but these are found to be important for controlling the water vapor distribution in the upper troposphere.

1. Introduction

Water vapor in the upper troposphere and lower stratosphere is an important radiatively active trace species. As a greenhouse gas, water vapor is important for determining the radiative balance of the upper troposphere, particularly in the tropics. This has implications for local diabatic heating and for feedbacks to climate radiative forcing [*Sun*, 1993; *Inamdar and Ramanathan*, 1998]. Because water vapor is a nearly conserved trace species in the stratosphere, with few significant sources and sinks, it is also important as a tracer for stratospheric transport.

As postulated by *Brewer* [1949] and recently reviewed by *Holton et al.* [1995] the water vapor distribution in the stratosphere is controlled by cold temperatures at the tropical tropopause. Air reaches saturation with respect to ice at the tropical tropopause and hence is "freeze-dried" as it crosses into the stratosphere. The motion of air across the tropical tropopause is affected by a variety of processes. These processes include the large-scale residual circulation in the stratosphere [*Rosenlof*, 1995] which cools air adiabatically and can cause it to reach saturation; overshooting convective turrets which penetrate the tropopause and either dehydrate [*Danielsen*, 1993] or rehydrate the air as condensed vapor evaporates [*Vömel et al.*, 1995]; subvisible cirrus clouds which may heat the tropopause through absorption of radiation [*Rosenfield et al.*, 1998], resulting in warmer temperatures and higher water vapor; and kelvin and gravity waves forced from the troposphere which may mix air into the stratosphere [*Pfister et al.*, 1993] or modify the local temperature structure, cooling air to the point of saturation and dehydration [*Potter and Holton*, 1995]. As noted by *Holton et al.* [1995], the relative importance of these processes for stratosphere-troposphere exchange in the tropics and the effects of each of these processes on water vapor in this region are still uncertain.

This uncertainty stems from the lack of sufficient observations in these regions. Observations of water vapor in the upper tropical troposphere and lower stratosphere have been increasing in recent years, but coverage is far from accurate or complete. The major sources of data are radiosondes (balloons), satellites, and aircraft. Radiosonde moisture measurements are often unreliable in the extreme dryness of the upper troposphere and lower stratosphere [*Gaffen*, 1999]. Satellite data are of better quality, but coarse horizontal

[1]Now at National Center for Atmospheric Research, Boulder, Colorado.

Paper number 1999JD901133.
0148-0227/00/1999JD901133$09.00

and especially vertical resolution, often sampling layers 1–3 km thick. Satellite data include observations from the Stratospheric Aerosol and Gas Experiment II (SAGE II) [*Pan et al.*, 1997], the Microwave Limb Sounder (MLS) [*Read et al.*, 1995; *Newell et al.*, 1996] on the Upper Atmosphere Research Satellite (UARS), and the Halogen Occultation Experiment (HALOE) [*Russell et al.*, 1993] also on UARS. Observations of high quality and spatial resolution are also available from in situ aircraft [*Boering et al.*, 1995; *Hintsa et al.*, 1998] and research balloons [*Ray et al.*, 1999], but these platforms provide limited spatial and temporal sampling.

In this study, we will simulate the water vapor distribution in the lower stratosphere and upper troposphere using a transport model with a parameterized hydrologic cycle. We will focus on the importance of thermodynamic processes and the global wind field. Convective turrets and small scale waves (such as gravity waves on horizontal length scales smaller than hundreds of kilometers) will not be included in the simulations. The significance of convection and gravity waves can be judged indirectly by their absence from the simulations. Good correspondence between simulations without these processes and observations will indicate that large-scale transport is more important, while systematic deviations between the simulations and observations indicate the importance of other processes which are not represented. It is possible that small-scale processes (such as convection and wave activity) may affect the water vapor concentration in opposite ways and even act to cancel each other, which would still indicate that these processes have no net impact on the water vapor distribution. The approach attempts to build upon the water vapor modeling work of *Mote et al.* [1994] and *Mote* [1995] which used a general circulation model (GCM) that included feedbacks and parameterized convection. Here we seek an approach which limits the number of simulated processes to better determine their relative importance.

The focus is on three regions. The first region is the lower stratosphere between the 380 K and 500 K potential temperature surfaces (isentropes). This region is approximately from the highest isentrope that does not lie in the tropical troposphere [*Holton et al.*, 1995; *Hoskins*, 1991] to the lower boundary of the "tropical pipe" region [*Plumb*, 1996]. The region above the 380 K surface is also known as the "stratospheric overworld" [*Holton et al.*, 1995]. The second region is the "extratropical lowermost stratosphere" [*Holton et al.*, 1995] also known as the stratospheric "middleworld" [*Hoskins*, 1991], which lies between the extratropical tropopause and the isentrope whose level is approximately equal to the tropical tropopause (380 K). The third region is the upper tropical troposphere. Transport between the stratospheric overworld and the troposphere occurs only across an isentrope (diabatic motion), while transport between the lowermost stratosphere and the troposphere may occur along an isentrope (quasi-isentropic motion). For a complete review see *Holton et al.* [1995].

The transport model and simulation parameters are described in section 2. Details of the temperature distribution are given in section 3. The simulated distributions of water vapor in the stratospheric overworld (above 380 K), in the middleworld, and in the upper tropical troposphere are detailed in section 4. Detailed comparisons with observations are presented in section 5. The stratosphere-troposphere exchange of water vapor is discussed in section 6. Discussion and conclusions are contained in section 7.

2. Description of Model and Constraints

The three–dimensional Chemical Transport Model (CTM) of the Laboratory for Atmospheres at the Goddard Space Flight Center (GSFC) is used for this analysis. The model accurately simulates the detailed distribution of chemical tracers including ozone [*Douglass et al.*, 1996] and carbon dioxide [*Strahan et al.*, 1998]. The CTM is fully described by *Douglass et al.* [1996], but key parameters are repeated here. The three-dimensional flux form semi-Lagrangian transport code [*Lin and Rood*, 1996] uses 46 level winds from the Goddard Earth Observing System (GEOS) Assimilation System [*Schubert et al.*, 1993]. The transport scheme is specifically designed for avoiding negative tracer values and for conserving mass. Model resolution is 2° latitude by 2.5° longitude with 46 hybrid sigma-pressure levels in the vertical from the surface to 0.1 hPa. The interface between sigma and pressure occurs at ~400 hPa, so that the region discussed in this work is all in pressure coordinates. The model pressure levels are ~20 hPa (1 km) apart near the tropical tropopause. The model is run in an off-line mode, so the tracer concentrations do not feedback to affect the winds and temperatures. Input winds and temperatures are interpolated to a 15 min (900 s) time step from 6 hourly assimilation data. Explicit convective transport is not included. Vertical motion is calculated from the divergence of the horizontal wind. *Douglass et al.* [1996] note two benefits of using an offline transport model over a full GCM with chemistry and feedbacks; the ability to have temperatures more representative of the actual stratosphere than those in most GCMs and to appropriately simulate individual synoptic-scale perturbations for comparison to observations. Both of these benefits are critical to the simulations described in this work and distinguish this analysis from the GCM study of *Mote et al.* [1994]. For comparison of the simulation with observations, a variety of assimilated and observed data sets are used. These data sets are discussed more fully as each is introduced; they range from global assimilation systems to individual radiosonde stations.

Several simulations of water vapor were performed. The results here are mostly drawn from an experiment designed to crudely represent the hydrologic cycle. A

tracer was initialized with a source of 5% of atmospheric concentration (50,000 parts per million by volume (ppmv)) at the surface. In the lower troposphere (from the surface to 400 hPa), a sink is parameterized by a 7 day e folding lifetime (relaxing to zero). Simulated tracer in the upper troposphere and above is not sensitive to the concentration at the ground using this parameterization of water vapor. From 400 to 80 hPa, the tracer is checked against the saturation vapor mixing ratio (SVMR or hereafter $\chi_{\rm sat}$) of water over ice at each time step using the algorithm of *Marti and Mauersberger* [1993]. This algorithm was chosen because it is based on experimental data down to 170 °K, covering the range of tropical tropopause temperatures commonly observed (see section 3). If the tracer concentration is larger than $\chi_{\rm sat}$, the tracer value is reduced to the saturation value. This process is analogous to the "dehydration" that occurs when water vapor passes from the vapor phase into either liquid or solid phase and then precipitates and occurs when the "relative humidity" in the simulation is 100%. In this work, we will repeatedly use the term "relative humidity". Relative humidity or "RH" is defined as:

$$\mathrm{RH} = \frac{\chi_t}{\chi_{\rm sat}(T,p)} 100, \qquad (1)$$

where χ_t is the model tracer or observed water vapor mixing ratio and the saturation vapor mixing ratio ($\chi_{\rm sat}$) is a function of the temperature T and pressure p according to *Marti and Mauersberger* [1993].

In another simulation which will be referred to as the "tropical" or "saturated" simulation, the tracer mixing ratio was fixed at the SVMR ($\chi_{\rm sat}$) from 157 to 94 hPa in the region from 10°S to 10°N with the tropospheric sink described above but with no surface source. This simulation tests the condition of a fully saturated upper troposphere and region of entry of air into the stratosphere.

The tracer, while referred to as the "water vapor tracer," is not necessarily comparable to the water vapor mixing ratio in the atmosphere. It will be comparable only if the major processes affecting water vapor are "dehydration" and transport. In particular, there is no source of water in the upper stratosphere, as occurs in the atmosphere from the oxidation of methane [*Brasseur and Solomon*, 1986]. An accurate simulation of water vapor in the middle and upper stratosphere should include this source. The methane concentration observed in the stratosphere [*Randel et al.*, 1998] falls from 1.6 ppmv at the tropopause to 0.2 ppmv at 50 km (1 hPa), indicating that 1.4 ppmv of methane is converted into ~3 ppmv of additional stratospheric water. Supersaturation is not permitted in the simulation. Processes that occur in and around clouds, such as reevaporation of falling liquid or solid H_2O, are also not treated. Differences between the simulation and observations will be discussed in light of these missing processes where appropriate.

The model is run for 3 years starting October 1, 1995, and repeating meteorology from October 1, 1995, to October 1, 1996, each year. The dates were based on the availability of a full year of continuous and consistent assimilation data at high vertical resolution. The climate of this year featured moderate La Nina conditions, with small cold anomalies in the Eastern Pacific (data available at http://www.cdc.noaa.gov). The Climate Prediction Center (CPC) at the National Centers for Environmental Prediction (NCEP) provides selected indicators of stratospheric climate for the winter season in each hemisphere (available at http://nic.fb4.noaa.gov). The CPC reports both Southern Hemisphere (SH) winters (1995 and 1996) featured cold temperatures and a strong vortex. The Northern Hemisphere (NH) winter of 1995–1996 was remarkably cold until spring with a strong vortex. These cold temperatures (which extended into the tropics) might be expected to result in especially low water vapor concentrations, which should be reflected in the GEOS analysis and hence in the simulations. Comparisons will be made with the same time period, so this should not complicate the analysis.

In the region of the atmosphere being studied (below 500 K), the transport lifetimes are generally 1 year or less, as shown by *Schoberl et al.* [1998], so all major timescales of variability are captured. There is a small secular increase in mixing ratios in the stratosphere which is evident in the overworld mass burden for water vapor. The increase is expected given the transport lifetimes in the stratospheric overworld. Since this analysis concerns itself with the lower stratosphere only (below the tropical pipe region at ~500 K), the 3 year duration should be sufficient. Most analyses here will use only the third year of data from the simulations, to compare with observations from the period October 1995 to October 1996.

3. Temperature Comparison

The only sink for water vapor outside of the lower troposphere in the simulation is a thermodynamic constraint that the tracer concentration be below the saturation vapor mixing ratio ($\chi_{\rm sat}$) of water over ice. Since the water vapor concentration in the tropical upper troposphere is typically close to $\chi_{\rm sat}$, temperature is a critical parameter for determining the water vapor distribution in the lower stratosphere and upper troposphere. For the simulation to represent the water vapor distribution correctly, accurate temperatures are a prerequisite.

Figure 1 illustrates the temperature distribution from the GEOS and the European Centre for Medium Range Weather Forecasts (ECMWF) analyses. Figure 1a illustrates zonal monthly mean temperatures for January 1996. The GEOS and ECMWF analyses reproduce the key temperature features in the upper troposphere and lower stratosphere, as described by *Schubert et al.* [1995]. The minimum of the temperature field in the

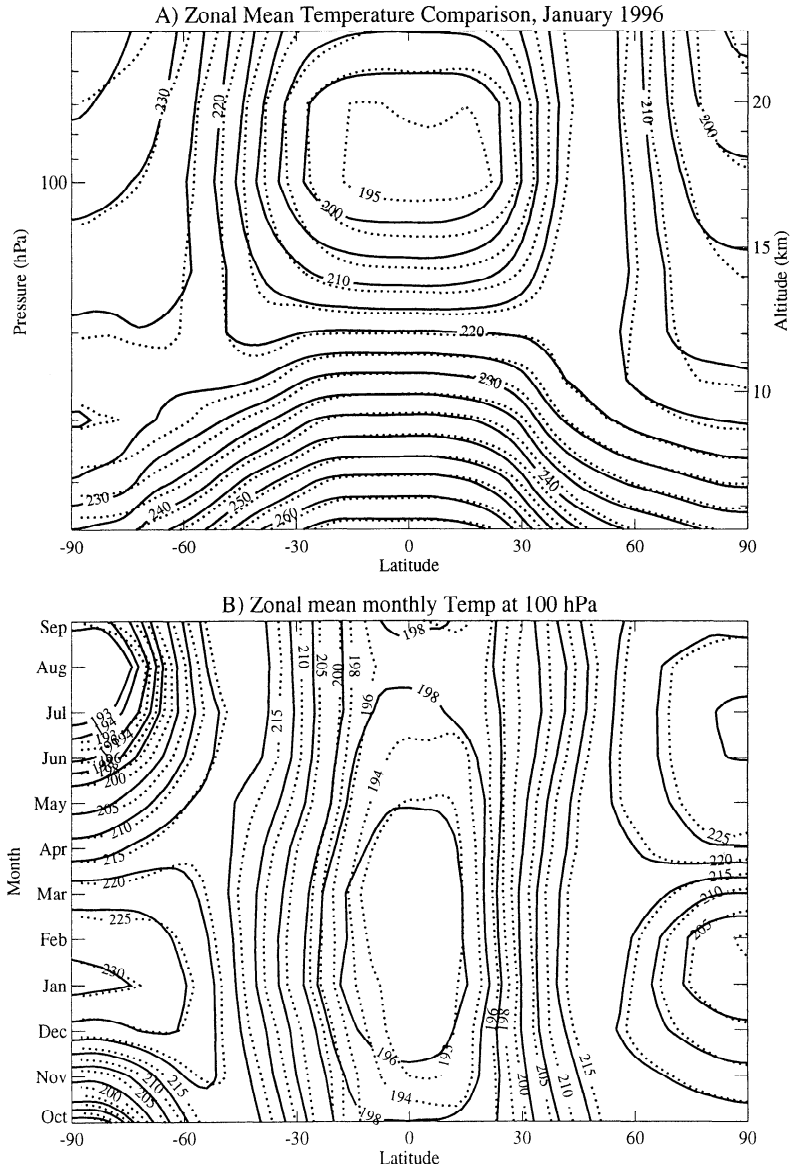

Figure 1. Zonal mean monthly temperature for (a) January 1996 (contour interval 5 °K) and (b) monthly at 100 hPa (contour interval 2 °K up to 200 °K, 5 °K thereafter, 193 °K also plotted for clarity). GEOS analyses are solid contours; ECMWF analyses are dotted contours.

tropics (the cold point) is usually at or slightly above the tropical tropopause, in agreement with radiosonde observations [*Reid*, 1998]. However, the GEOS temperatures are 3–4 °K warmer than ECMWF temperatures at the cold point (100 hPa) in January and throughout much of the year (Figure 1b). The difference increases from virtually identical mean temperatures at the 200 hPa level (Figure 1a). Similar differences at the tropical tropopause have been found by *Schubert et al.* [1995] and *Pawson and Fiorino* [1999] using GEOS and ECMWF reanalyses for many years. GEOS analyses are also 2–3 °K warmer than NCEP analyses at the tropical tropopause (not shown). *Pawson and Fiorino* [1999] note that ECMWF analyses agree more closely with radiosonde data, and they attribute the warmer tropical tropopause temperatures in the GEOS assimilation to the strong weighting given satellite radiances in the GEOS assimilation. ECMWF assimilations give more weight to the colder radiosonde data.

This temperature difference may have some profound effects on stratosphere-troposphere exchange of water vapor in the simulation. For a sample location at 191 °K and 100 hPa, increasing the temperature by 2 °K will increase χ_{sat} by nearly 40% (from 3.9 to 5.5 ppmv). For temperatures as high as 210 °K, a 2 °K change in temperature represents a 25% difference in χ_{sat}.

Zonal temperature variations in the tropics are important for discussions of regions where there is preferential upward mass flux, the "stratospheric fountain" hypothesis of *Newell and Gould-Stewart* [1981]. There is a zonal asymmetry in upper tropical tropospheric temperatures, specifically at 94 hPa, the level of max-

imum simulated dehydration in the NH winter season. Minimum temperatures generally occur over the Pacific from 120° to 180°E and from 20°N to 10°S. These temperatures are 2–3 °K colder than those in other regions in the NH winter. In the NH summer from May to September, temperatures are more zonally symmetric than in the NH winter. In the NH summer the longitudinal variation of temperature is <1 °K at the cold point over the tropics. The zonally averaged 100 hPa temperature is ~4 °K lower in February than August, in rough agreement with analyses by *Pawson and Fiorino* [1999].

4. Simulated Water Vapor Distribution

The monthly averaged zonal mean simulated water vapor tracer reproduces major features of the water vapor concentration of the lower stratosphere and upper troposphere as depicted in Figure 2 for January in the third year of the simulation, corresponding to January 1996. There is a minimum in the tracer concentration just above the tropical tropopause where cold temperatures dehydrate the air. The tracer concentrations are high in the tropics and lower in the extratropics in the middle stratosphere. The meridional gradients in the lowermost stratosphere (below 100 hPa) are very flat, suggesting rapid horizontal (quasi-isentropic) transport and mixing across the tropopause. This may be misleading since water vapor is not a conserved quantity in this region and hence does not act as a tracer for transport. There is a water vapor sink in the tropical upper troposphere preventing the formation of sloping isopleths. There is a sharp jump in the tracer concentration in the middle and high latitudes just below the tropopause (~8 km). The Southern Hemisphere (summer) middleworld has slightly higher concentrations than the Northern Hemisphere (winter) middleworld. Except at the tropical tropopause, the tracer concentration decreases steadily with altitude from the surface source.

A focus on the entry of air into the stratosphere is presented for the 3 years of the simulation in Figure 3. There is a maximum in the tropics in September in each hemisphere, which takes 3–4 months to propagate to high latitudes. The tropical maximum is more pronounced in the Northern Wemisphere. The tropical maximum does not appear to propagate as readily into the high latitudes of the Southern Hemisphere, also seen in analysis of water vapor observations from HALOE by *Rosenlof et al.* [1997]. The annual cycle in the high latitudes in the Southern Hemisphere is due to the annual cycle of temperatures in this region which dehydrate the air at cold winter temperatures. However, the high water vapor values in austral fall and winter (April to July) are partly due to difficulties in accounting for extremely low surface pressures at high latitudes. Transport on a near coincident potential temperature (θ) surface indicates similar patterns.

4.1. Tropical Tape Recorder

The tropical stratospheric "tape recorder" discussed by *Mote et al.* [1996] is also present in the water vapor simulation. The tape recorder signal is easily seen in the

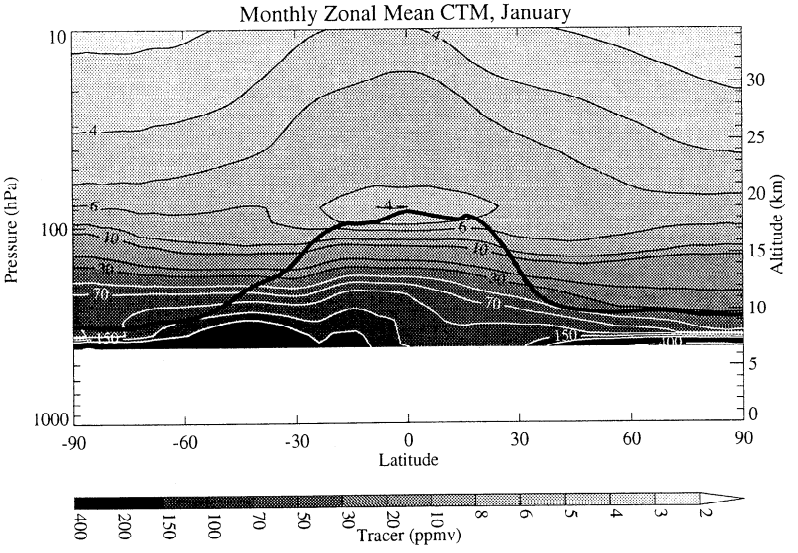

Figure 2. January monthly zonal mean tracer mixing ratio for the third year of simulation, in units of ppmv. Thick solid line is the monthly mean tropopause for January 1996 calculated using the 3 PVU (Potential Vorticity Unit) potential vorticity surface, and 380 K potential temperature surface in the tropics. 1 PVU = 10^{-6} K kg^{-1} m^2 s^{-1}.

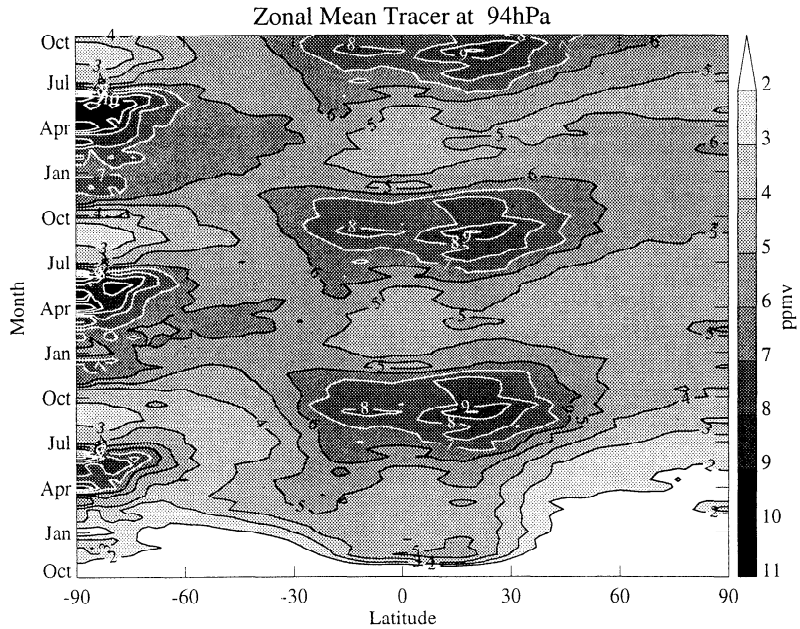

Figure 3. Zonal mean tracer mixing ratio at 94 hPa for 3 years, in units of ppmv.

zonal mean water vapor concentration at the equator, presented in Figure 4. The annual cycle of the water vapor tracer at 94 hPa seen in Figure 3, which corresponds to the annual variation in cold point temperatures [*Yulaeva et al.*, 1994], propagates vertically in the stratosphere. In the simulation the speed of the tape recorder (vertical transport) is much too rapid. The propagation time of the signal from 100 to 50hPa is less than 3 months. The observed tape signal as illustrated by *Mote et al.* [1996] with data from MLS or HALOE (both on UARS) takes of the order of 6 months to transit this region. Rapid vertical transport using GEOS winds has also been noted by *Strahan et al.* [1998] for a simulation of CO_2 in the stratosphere and by *Hall et al.* [1999] in an intercomparison of tracer transport in many stratospheric models.

The seasonality of the source function is approximately correct. The highest observed water vapor mixing ratios from UARS instruments at 100 hPa reported by *Randel et al.* [1998] of ~4.5-5 ppmv are seen in August to October, and the lowest observed mixing ratios of ~2.5-3 ppmv) occur in January to April (compare to

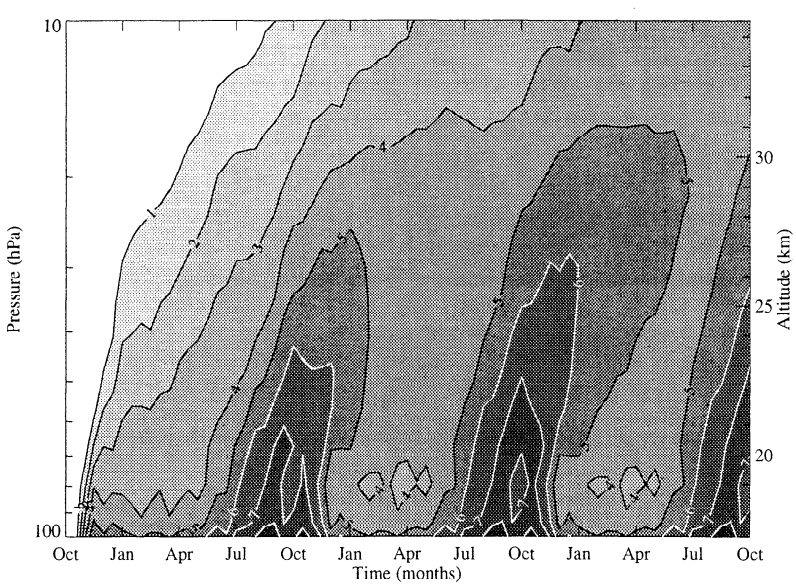

Figure 4. Zonal mean tracer mixing ratio at the equator in units of ppmv.

Figure 3). The minimum tracer concentrations occur above 100 hPa, at approximately the same altitudes as minima observed from satellite data [*Mote et al.*, 1996]. The amplitude of the tape recorder signal of ~3 ppmv is similar to that observed with UARS instruments (2–3 ppmv). The maximum amplitude is simulated at approximately the correct altitude (just above 100 hPa). The simulated tape recorder appears to well represent the "recording head" at the tropical cold point, recognizing the warm bias in temperature, while the signal propagation in the vertical appears too fast. The signal attenuation is also too rapid compared to observations. A noticeable signal in water vapor is clearly evident to at least 30 km, similar to the altitude observed by *Mote et al.* [1996]. However, since the signal is attenuated too fast relative to observations [*Mote et al.*, 1996], there is more meridional mixing in the stratosphere in the simulation than in the real atmosphere.

4.2. Water Vapor Mass Burden

The water vapor mass in the Southern Hemisphere, the Northern Hemisphere, and the tropics is calculated by converting the tracer mixing ratio into mass for each grid cell and then dividing the tracer mass into regions using potential vorticity and potential temperature surfaces from archived 18 level GEOS assimilation data. The daily mass of water vapor tracer in the lower stratospheric overworld (380–500 K), the middleworld (Tropopause to 380 K), and the tropical troposphere is illustrated in Figure 5. Note that the data is unsmoothed and the mass burdens change slowly over the year in all regions, with small day to day variability.

In the lower stratosphere (Figure 5a) the seasonal cycles of the tracer burden in the NH and SH extratropics are out of phase, and both hemispheres have their largest mass of water vapor tracer in the late summer (February-March in the SH, August in the NH) and minima in winter (August in the SH, January in the NH). A linear trend from the continued increase of tracer in the lower stratosphere is present in the overworld burden (Figure 5a). The trend is easier to observe in Figures 3 and 4. By year 3 in the simulation, this trend is less than a 10% annual increase in the tracer burden as the stratosphere continues to adjust toward equilibrium from the initial zero distribution. The annual average reservoir in the NH has 10% more water vapor than the Southern Hemisphere. A "moister" NH is consistent with warmer tropical temperatures in NH summer (see Figure 1b), when the tropical upwelling region is north of the equator (see Figure 3) and a larger annual cycle is in high latitudes of the Southern Hemisphere (a result of dehydration in the SH under cold temperatures). This interpretation is consistent with the findings of *Rosenlof et al.* [1997].

The tropical ($|\phi| < 20°$) reservoir in the stratospheric overworld (Figure 5a, dotted line) is in approximate phase with the Northern Hemisphere reservoir. The mass of water vapor tracer is lowest in NH winter and highest in NH late summer (August–September). This agrees with the cycle of mixing ratios noted in section 4.1. The phase of the seasonal cycle in the tropical stratospheric overworld is not sensitive to the latitude chosen as the edge of the tropical boundary.

The reservoir of water vapor in the stratospheric middleworld (also called the extratropical lowermost stratosphere), illustrated in Figure 5b, indicates in the annual average that the NH has 10% more tracer mass than the SH. This convolves the size of the middleworld with the concentration. The annual cycle of middleworld mass is simpler in the SH where the annual mass of the middleworld does not change much over the year [*Appenzeller et al.*, 1996]. The SH middleworld mass of tracer is high in summer (January to March) and low in winter (July to October). The NH middleworld tracer burden is a maximum in June and a minimum in February. The NH middleworld air mass works against this cycle in tracer mass, being low in July to September and high in December to March.

The tracer mass in the tropical troposphere (Figure 5c) has a distinct annual cycle in each hemisphere above 400 hPa. The tropical water vapor mass is higher in summer than in winter in each hemisphere (see section 4.5 for further discussion). The NH has a larger tropospheric mass of water vapor than the SH. The compensation between the summer and winter hemispheres keeps the total water vapor mass in the tropical troposphere within ±4% of the annual mean throughout the year. Note that the total mass (due to higher mixing ratios and pressures) is 3 orders of magnitude (10^{21} kg) larger than in any region of the stratosphere (Figures 5a and 5b).

4.3. Relative Humidity

The distribution of "relative humidity" (see Equation 1), shows that the maximum humidities away from the surface source occur around the tropopause and in the stratospheric winter polar vortex in the Southern Hemisphere between 20–30 km (Figure 6). Note that dehydration is still occurring at levels when the zonal mean humidity is <100% since the zonal mean is an average. The zonal mean picture is a convenient way to examine where saturated conditions for the simulated tracer occur. In the winter polar regions, dehydration occurs in both hemispheres. Colder temperatures in the Southern Hemisphere result in dehydration at up to 40 hPa (Figure 6b), while in the Northern Hemisphere, dehydration occurs mostly below 100 hPa (Figure 6a).

Air is closer to saturation at 94 hPa in February (NH winter) than August, consistent with the annual cycle of tropical temperatures [*Yulaeva et al.*, 1994]. The zonal mean RH of the tracer at 94 hPa in tropics is typically 65% in August and 70% in February. The standard deviation in space (latitude and longitude) of the relative humidity in the tropics at this level is ~20% at any time. The relative humidity generally reaches a local maximum in the extratropics around the altitude of the

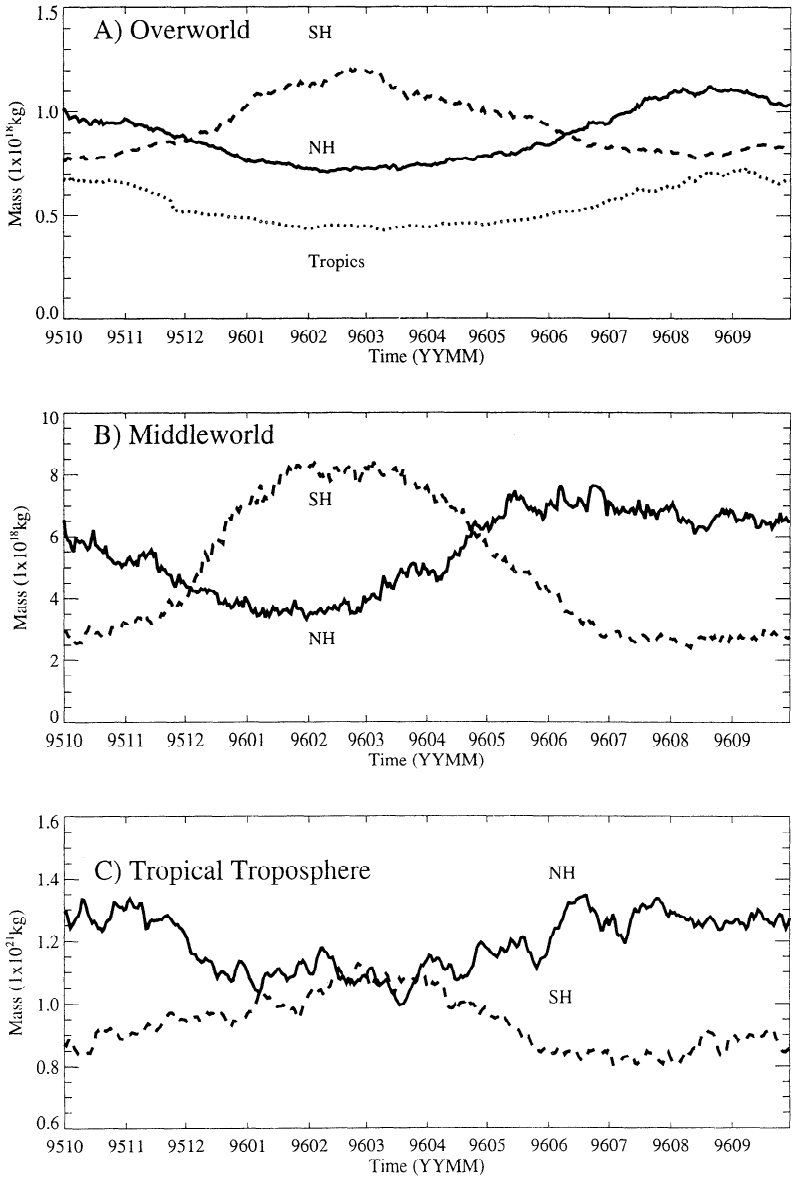

Figure 5. Hemispheric mass budgets for water vapor tracer. (a) Lower stratospheric overworld between 380 K and 500 K. Here 20°–90°N is represented by a solid line, 20°–90°S by a dashed line, and 20°S–20°N by a dotted line. (b) Stratospheric middleworld (between 3 PVU tropopause and 380 K surface). Here 20°–90°N is represented by a solid line and 20°–90°S by a dashed line. (c) Tropical Troposphere (400 hPa to the tropopause). Here 0°–20°N is represented by a solid line and 20°S–0° by a dashed line.

tropopause. In this simulation the maximum RH in the tropics corresponds to the maximum removal of tracer owing to concentrations higher than the local χ_{sat}. The maximum RH (Figure 6) occurs around 180 hPa in the summer hemisphere, though significant regions of saturated conditions occur up to the cold point at 94 or 79 hPa, especially in February. Air in this simulation generally reaches saturation at altitudes well below the cold point (though it may be saturated up to the cold point), and air entering the stratosphere in the tropics is not always saturated.

The lower stratosphere and upper troposphere have very different zonal distributions of relative humidity. In the tropical lower stratosphere (100–80 hPa) the relative humidity is zonally symmetric. Relative humidity of the simulated tracer at 94 hPa is generally between 60 and 80% in all seasons. In the upper troposphere (220 hPa), RH is zonally asymmetric. RH in December through March ranges from 20% in the Eastern Pacific (180°–270° longitude) to 60-80% over the Maritime Continent (90°–130° longitude) at 220 hPa. A similar zonal asymmetry is also clear in August during the active period of the Asian monsoon. In the upper troposphere, the pattern is consistent with the tropical Walker circulation [*Bjerknes*, 1969] of rising air over Indonesia and South America bringing moisture from

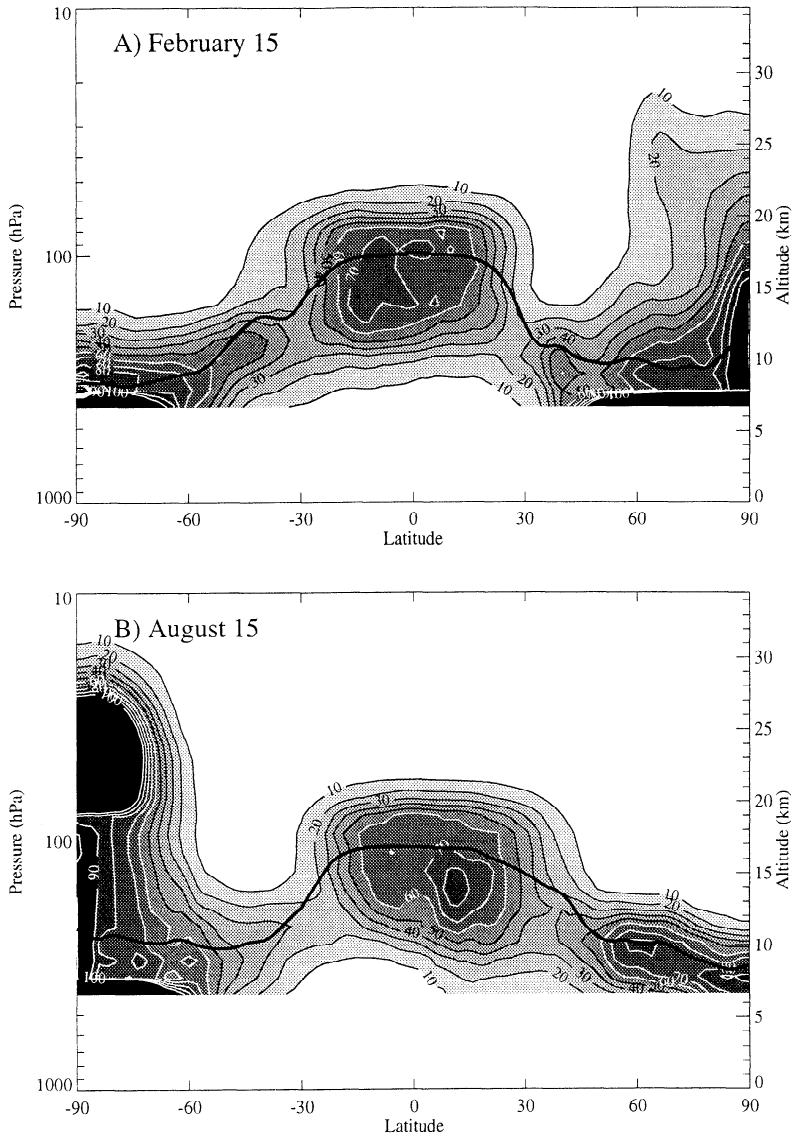

Figure 6. Zonal mean tracer "relative humidity" (see Equation 1) in percent for (a) February 15 and (b) August 15. Solid black line is the zonal mean daily 3 PVU tropopause surface.

the lower troposphere and sinking air over the Eastern Pacific from the upper troposphere/lower stratosphere where the air has experienced cold temperatures and been dehydrated and then warmed. See section 4.5 for more discussion of the upper troposphere.

4.4. Middleworld

The water vapor tracer in the extratropical lowermost stratosphere (middleworld) has a defined annual cycle (Figure 7), low in the winter season in both hemispheres and high in the summer season. In the Northern Hemisphere, the high-latitude maxima occur 2–3 months after a significant increase in averaged mixing ratio in the tropics. In the Southern Hemisphere, the signal is less clear, and a broad high-latitude maximum is present from January through April. This maximum is coincident with the appearance of a maximum in the tropical troposphere south of the Equator. Because of changing tropopause heights and the changing size and altitude of the middleworld, it is perhaps more useful to view the data in isentropic coordinates, following *Pan et al.* [1997]. Figure 8 presents the zonal mean mixing ratio at 50° in both hemispheres on isentropic surfaces for the third year of the simulation. Only locations in the stratosphere (as defined by potential vorticity) are averaged. There is a strong vertical gradient in the lowermost stratosphere (up to 380–400 K), with a defined annual cycle which is generally confined to the lowermost stratosphere. The annual cycle has a broad maximum between June and September below 350 K in the Northern Hemisphere and a smaller maximum from January to March at these altitudes in the Southern Hemisphere.

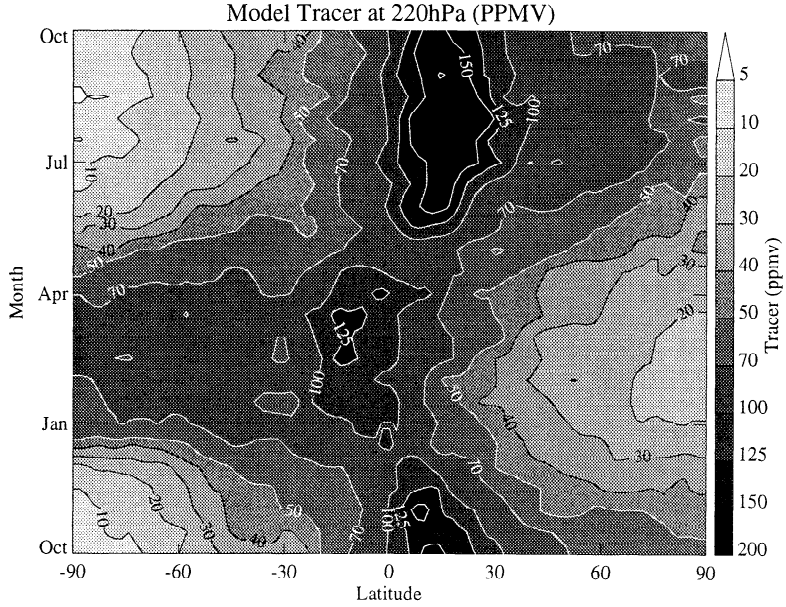

Figure 7. Zonal mean tracer mixing ratio at 220 hPa in units of ppmv for third year of the simulation.

The Northern Hemisphere middleworld is moister than Southern Hemisphere in midlatitudes, when viewed either by mixing ratio (Figure 7 and Figure 8) or by total mass of the vapor tracer (section 4.2). The increased water vapor is particularly noticeable in summer, when there is a significant plume of tracer advected from the surface into the upper tropical troposphere and then quasi-isentropicly into the middleworld due to the monsoon circulation, which injects a large mass of water vapor tracer into the NH middleworld. A separate global simulation with a source of water vapor in the upper tropical troposphere but without a surface source of water vapor showed that without this plume of moist air, the Southern Hemisphere middleworld has higher tracer concentrations than the Northern Hemisphere. The time and spatial distribution of a plume of "dry" air from the surface in this simulation matches the seasonality and location of the South Asian, African, and North American monsoon circulations in the tropics. The monsoon penetrates more into midlatitudes in the Northern Hemisphere summer upper troposphere, causing the NH middleworld to receive a significant flux of air recently in the lower troposphere, moist air in the simulation with a surface source, and dry air in the simulation without a surface source. In the simulation with a surface source of water vapor tracer, as in the atmosphere, the effect of the monsoons is to moisten the Northern Hemisphere more than the Southern Hemisphere. The monsoon circulations are thus important for the annual cycle of water vapor in the lowermost stratosphere, as noted by *Rosenlof et al.* [1997].

4.5. Tropical Troposphere

The water vapor tracer concentrations in the upper tropical troposphere at 220 hPa have a clear annual cycle, depicted in Figure 7. Water vapor tracer concentrations are high in the summer subtropics in both hemispheres, and the maximum is not on the equator but rather migrates based on the movement of the Intertropical Convergence Zone (ITCZ) and monsoon circulations (for a description of the annual cycle of the ITCZ and monsoons see *Hartmann* [1994]). The zonal distribution of water vapor tracer in the upper troposphere at 220 hPa (Figure 9) has generally high values over South America and over the Maritime continent and low values over the eastern Pacific, consistent with the Walker circulation (seen also in the relative humidity fields in section 4.3). Zonal sections in time (Figure 9) illustrate eastward propagation of high and low anomalies with periodicity of 60 days or so. Similar patterns and signals in the MLS water vapor data have been noted by *Clark et al.* [1998], which they attribute to the Madden-Julian Oscillation (MJO). The MJO [*Madden and Julian*, 1994; *Clark et al.*, 1998] is one of the major modes of variability in the tropical troposphere. The MJO describes the organization of convection into active and inactive phases with a period of 30–60 days which propagate eastward and are strongest in the Indian Ocean and Western Pacific. This manifests itself in the upper tropospheric water vapor fields as an alternating high (active convection) and low (inactive convection) signal. The MJO is also found in zonal wind and surface pressure fields across the tropics. The appearance of the signal in the water vapor tracer (seen most clearly in Figure 9 from December to April) is thus related to realistic patterns of convergence and divergence from these assimilated fields. There is also some evidence of westward propagating anomalies from the region of high water vapor associated with the summer monsoon from 90°–0°E, which may be related

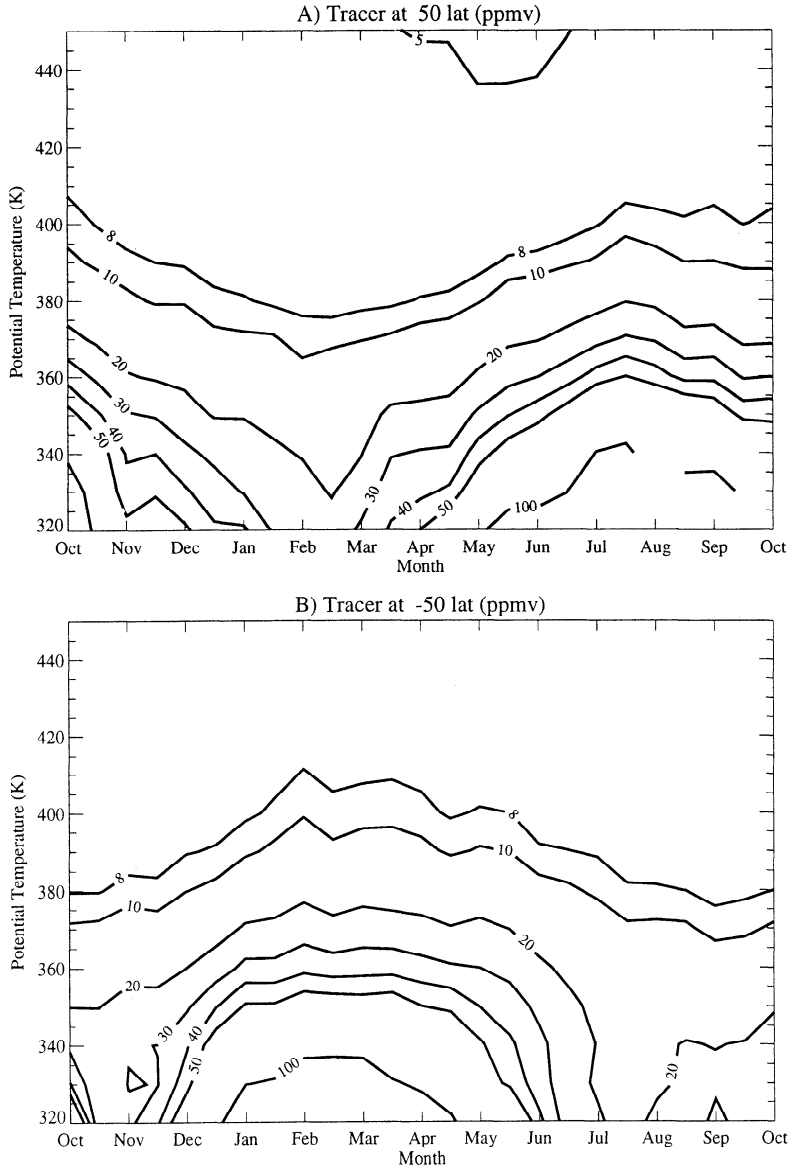

Figure 8. Zonal mean tracer mixing ratio on isentropic surfaces in the stratosphere (|Potential Vorticity| $> 3 \times 10^{-6}$ K kg^{-1} m^2 s^{-1}) in units of ppmv, evaluated twice a month. (a) 50°N and (b) 50°S.

to gravity wave activity [*Gill*, 1982, p. 452] associated with monsoon convection, as postulated by *Potter and Holton* [1995]. Further analyses are necessary to understand these smaller-scale patterns.

5. Comparisons With Observations

Because the simulation has no source of stratospheric water vapor, the tracer concentration decreases with height in the stratosphere. In the atmosphere, however, the oxidation of methane (CH_4) is a source of water vapor. Accordingly, only the lower stratospheric overworld and below can be compared to observations. In this section, a variety of satellite and radiosonde water vapor data are used for comparison.

A direct comparison of simulated tracer concentrations in the stratospheric overworld and water vapor data from the HALOE instrument on UARS [*Randel et al.*, 1998] is illustrated in Figure 10. The annual cycle of mixing ratio in the simulation illustrated in Figure 10 (and is also clear in Figures 3 and 4). The minimum in the simulated equatorial concentration of water vapor at 94 hPa appears in March, while the HALOE data have a minimum at 100 hPa in May. The tropical maximum in HALOE water vapor occurs in September or October, but the tropical maximum in the simulated tracer occurs in August. The difference may be due to the vertical weighting function of the HALOE data over ~2 km in the vertical, which smears out the arrival of the minimum at a particular altitude, and to differences in vertical transport in the simulation, which are discussed in section 4.1. It is likely that the latter is more important since the simulated minimum and maximum occur before the extrema in the HALOE observations,

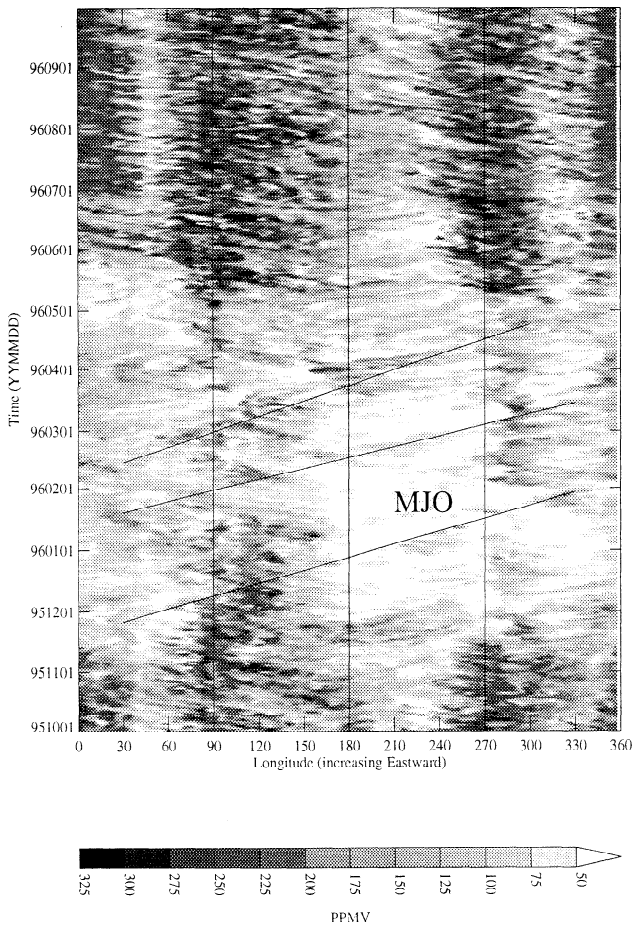

Figure 9. Hovemuller plot of daily tracer mixing ratio on 220 hPa at 10°N for 1 year in units of ppmv. Angled thin solid lines indicate approximate phase of high tracer concentrations with propagation resembling Madden Julian Oscillation (MJO) water vapor anomalies (see text).

consistent with stronger vertical velocities. At 100 hPa, the mean simulated tracer in the lower stratosphere is generally higher than HALOE water vapor concentrations by ~1–2 ppmv in NH winter and reaching 4 ppmv in NH summer. Given the possible temperature biases discussed in section 3, this difference is not surprising. An increase from 190 °K to 193 °K at 100 hPa corresponds to an increase in water vapor saturation mixing ratio of 2.2 ppmv, and an increase from 195 °K to 198 °K at 100 hPa increases χ_{sat} by 4.6 ppmv. It is difficult to compare the high-latitude data due to lack of HALOE coverage. Analysis of the HALOE data by latitude (not shown) indicates that at 100 hPa the NH polar minimum occurs in June, 3 months after the tropical minimum at 100 hPa and slightly slower than in the simulation at these altitudes (Figure 3).

The total hydrogen budget of the stratosphere is governed primarily by the mean value of methane and water vapor [*Mote et al.*, 1996]. The simulated value for the annual average water vapor entry into the stratosphere (~100 hPa at the equator) of 5–6 ppmv is higher than observed values from satellites, radiosondes, and in situ aircraft of ~4 ppmv, as illustrated in Table 1. The annual averaged minimum value in the simulated tracer actually falls at 79 hPa in the tropics, with the same annual cycle as illustrated at 94 hPa in Figure 10. The difference in the altitude of the minimum is related to the model resolution and the rapid vertical transport. Table 1 also illustrates the corresponding temperature at 80% relative humidity, approximately the highest average RH simulated in the tropics (Figure 6). While the simulation is considerably moister than previous observations from satellites, radiosondes or aircraft data, the differences correspond to differences in saturation temperatures of only 1°–3°C. This temperature difference

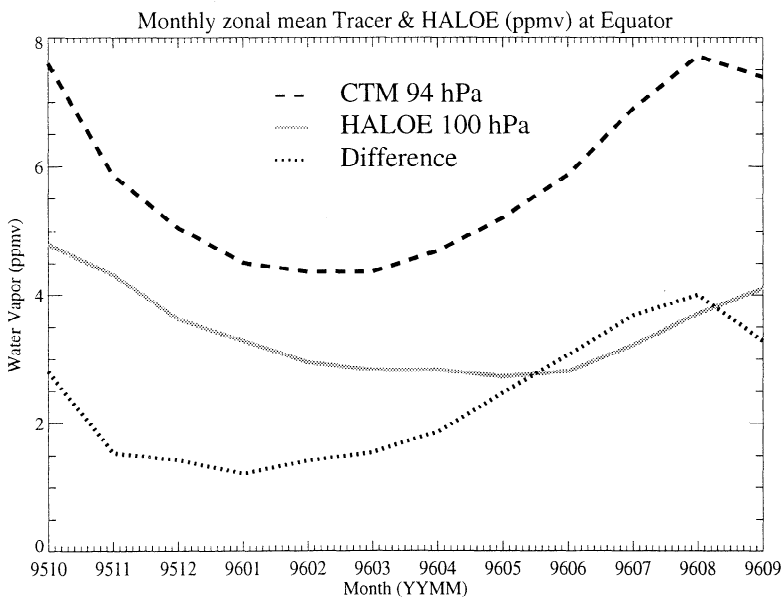

Figure 10. Monthly zonal mean HALOE water vapor mixing ratio and simulated tracer mixing ratio in units of ppmv at the equator. CTM Tracer at 94 hPa (dashed black line) and HALOE data at 100 hPa (solid grey line) are shown. Dotted line is the difference between them (CTM−HALOE). HALOE data are fully described by *Randel et al.* [1998].

Table 1. Annual Average Water Vapor "Entry" Mixing Ratio

Source	Reference	Pressure, hPa	Mixing Ratio, ppmv	Saturation Temp, °K
Model	This study	79	5.17	192.6
Model	This study	94	5.79	194.3
HALOE	*Randel et al.* [1998]	100	3.43	191.6
Radiosondes	*Dessler* [1998]	min χ_{sat}	3.8±0.3	192.2±0.5
ER2	*Hurst et al.* [1999]	100	4.0±0.3	192.5±0.5

Results from *Dessler* [1998] are reported at the minimum saturation vapor mixing ratio of each radiosonde (the average height of these minima is 98 hPa). Saturation temperature is based on average 80% relative humidity using the algorithm of *Marti and Mauersberger* [1993].

is of similar magnitude to the warm bias of the assimilation data as examined in section 3 and by *Pawson and Fiorino* [1999].

The phase of the annual cycle of water vapor in the middleworld (Figures 5b, 7, and 8) is similar to that observed by satellites and in situ platforms, but the absolute concentrations of the tracer are higher than observed water vapor mixing ratios in the middleworld. The annual cycle of water vapor in the middleworld (Figure 8) has the same phase as the cycle derived from SAGE-II water vapor data [see *Pan et al.*, 1997, Figures 4 and 5], with a broad maximum between June and September below 350 K in the Northern Hemisphere and a smaller maximum from January to March at these altitudes in the Southern Hemisphere.

The absolute value of the tracer on the 350 K potential temperature surface is generally higher than than the summer maxima of 10 ppmv in the NH and 5 ppmv in the SH reported by *Pan et al.* [1997]. As a result the amplitude of the seasonal cycle at 350 K in the simulation is 60 ppmv in the NH and 35 ppmv in the SH (Figure 8), while SAGE-II data have amplitudes of only 5 ppmv in the NH and 3 ppmv in the SH [*Pan et al.*, 1997]. Differences between simulated tracer values and SAGE-II water vapor concentrations are not surprising given more rigorous selection criteria for stratospheric points used by *Pan et al.* [1997]. SAGE-II data also have a dry bias since it only samples well away from cloudy regions [*Pan et al.*, 1997].

In situ measurements provide better accuracy but with more limited sampling. *Hintsa et al.* [1998] report in situ water vapor measurements from aircraft of 12–4 ppmv from 370–385 K in May in Northern Hemisphere midlatitudes (compared to 14–7 ppmv in May at 370–385 K in the simulated tracer at 50°). *Ray et al.* [1999] report balloon-borne in situ measurements of water vapor in the lowermost stratosphere at 35°N for 340–360 K of 30–15 ppmv in September (simulated tracer is 100–40 ppmv for the same location in September) and 20–10 ppmv in May (simulated 45–20 ppmv).

The amplitude and phase of the annual cycle in the simulated tracer in the upper tropical troposphere correspond to tropical MLS water vapor. Note that because MLS is a microwave instrument, it is able to see through clouds and sense only vapor [*Read et al.*, 1995], which makes it a good instrument for comparisons. Zonal mean model and MLS mixing ratios both indicate minimum water vapor concentrations in the NH subtropics during February (Figure 11a) and in July through October in the Southern Hemisphere (Figure 11b). Simulated tracer data have a wet bias in both hemispheres relative to MLS data at 215 hPa. Part of the bias results from the lack of signal in the MLS retrieval at low concentrations [*Read et al.*, 1995], which brings down the zonal mean. The phasing of the concentration maximum appears to be nearly synchronous between the simulation and MLS in both hemispheres. In the tropics (Figure 11c) the simulation shows excellent correspondence with MLS data, except during a dry period in April and May at the equator (also evident in Figure 7). This difference at the equator occurs in the simulation when the Eastern Pacific (180°–240°E) and South America (270°–330°E) dry out in April and May (not shown). Little change occurs during April and May in equatorial water vapor in the Western Pacific (90°–150°E) in the simulation or the observations. The cause of the difference is likely the failure of the simulation to resolve the convergence and divergence associated with convection over South America in April and May. With this exception, the amplitude and timing of the annual cycle are well represented by the simulation. Differences in the extratropics are thus a result of either differences in transport characteristics or differences in the water vapor mixing ratio in the stratospheric overworld. Given the known temperature bias and high entry level mixing ratio in the stratospheric overworld, it seems likely that the latter is important, although differences in transport cannot be ruled out.

Correspondence with MLS data is not limited to the zonal mean distribution. Daily point to point (5° latitude by 10° longitude) linear correlations between simulated tracer and MLS in the tropics and subtropics at 215 and 146 hPa are around 0.7, significant at well beyond the 99% confidence level (these correlations include several hundred points daily). In the extratropics, the correlations are lower (0.5) but still significant at the 99% level. These correlations indicate that synoptic scale variability is well represented.

Simulated tracer concentrations can also be compared to radiosonde observations. Since radiosonde observa-

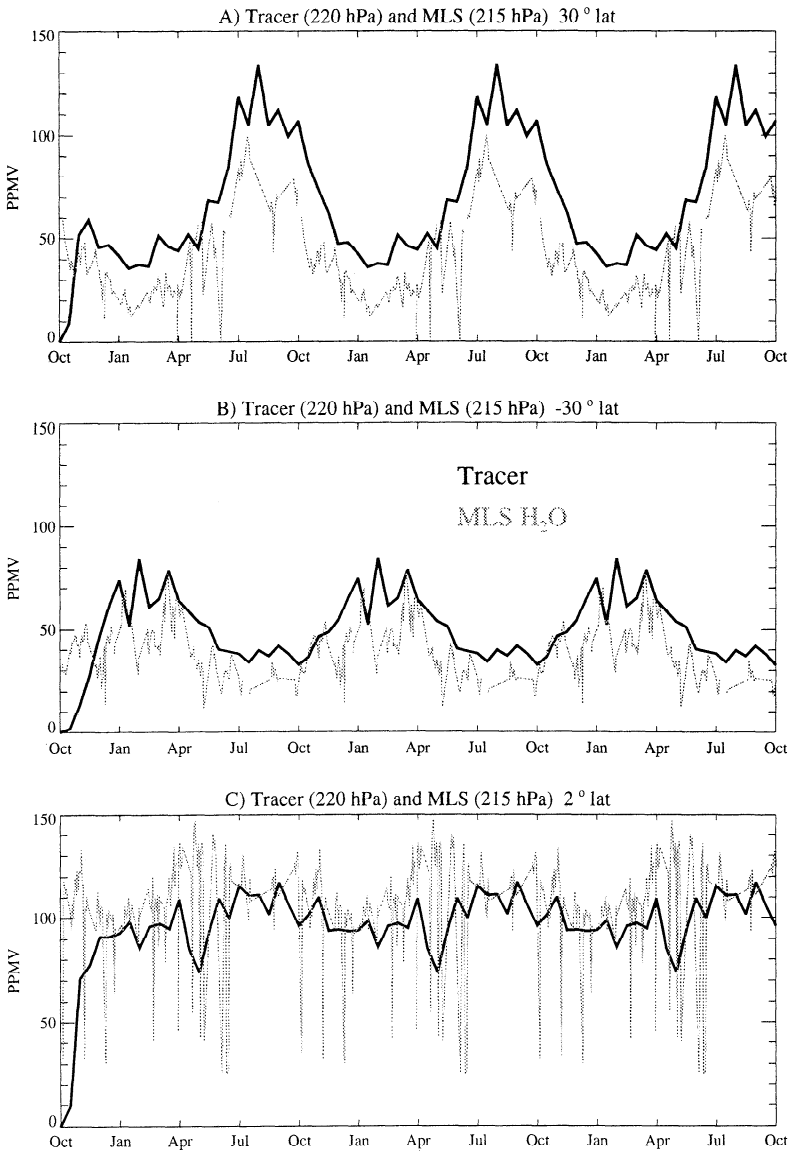

Figure 11. Zonal mean tracer mixing ratio at 220 hPa (thick black line) and MLS water vapor mixing ratio at 215 hPa (thin grey line) in units of ppmv. (a) 30°N, (b) 30°S, (c) 2°N are shown. MLS data from October 1995 to October 1996 repeated 3 times for comparison with 3 year tracer record.

tions of humidity in the upper troposphere and lower stratosphere are not of research quality [*Gaffen*, 1999], radiosonde temperature measurements were converted to saturation vapor mixing ratio (χ_{sat}) and compared to simulated χ_{sat} and simulated tracer values. Figure 12 presents an analysis for Koror, an island station in the Western Pacific (8°N, 135°E) and the model grid point containing Koror. Two other nearby island stations in the Western Pacific, Yap (9°N, 138°E), and Ponape (7°N, 158°E) have distributions almost identical to Koror. Several tropical and subtropical stations at other longitudes (Diego Garcia in the Indian Ocean, Hilo in the Central Pacific, and Barbados in the Atlantic) were also examined. Model fields for χ_{sat} and tracer were interpolated to radiosonde mandatory reporting levels. Generally, simulated χ_{sat} reproduces the annual cycle at Koror at 80 hPa (Figure 12a) and at 250 hPa (Figure 12d), but significant differences exist between these altitudes (Figures 12b and 12c). The χ_{sat} values calculated using radiosonde temperatures and using assimilated temperatures have similar ranges at 80 hPa and 250 hPa but are different at 100 hPa and 150 hPa. The simulated relative humidity (tracer nearly equal to χ_{sat}) is highest at 150 hPa, consistent with Figure 6. In Figure 12d at 250 hPa the tracer is far below saturation, with relative humidities of ~30% in February and ~50% in August, in agreement with Figure 6.

At 100 hPa (Figure 12b) and 150 hPa (Figure 12c) the simulated χ_{sat} is significantly higher than χ_{sat} estimated using radiosonde temperatures throughout the year, consistent with the warm bias of assimilation temperatures at the cold point discussed in section 3. At 80

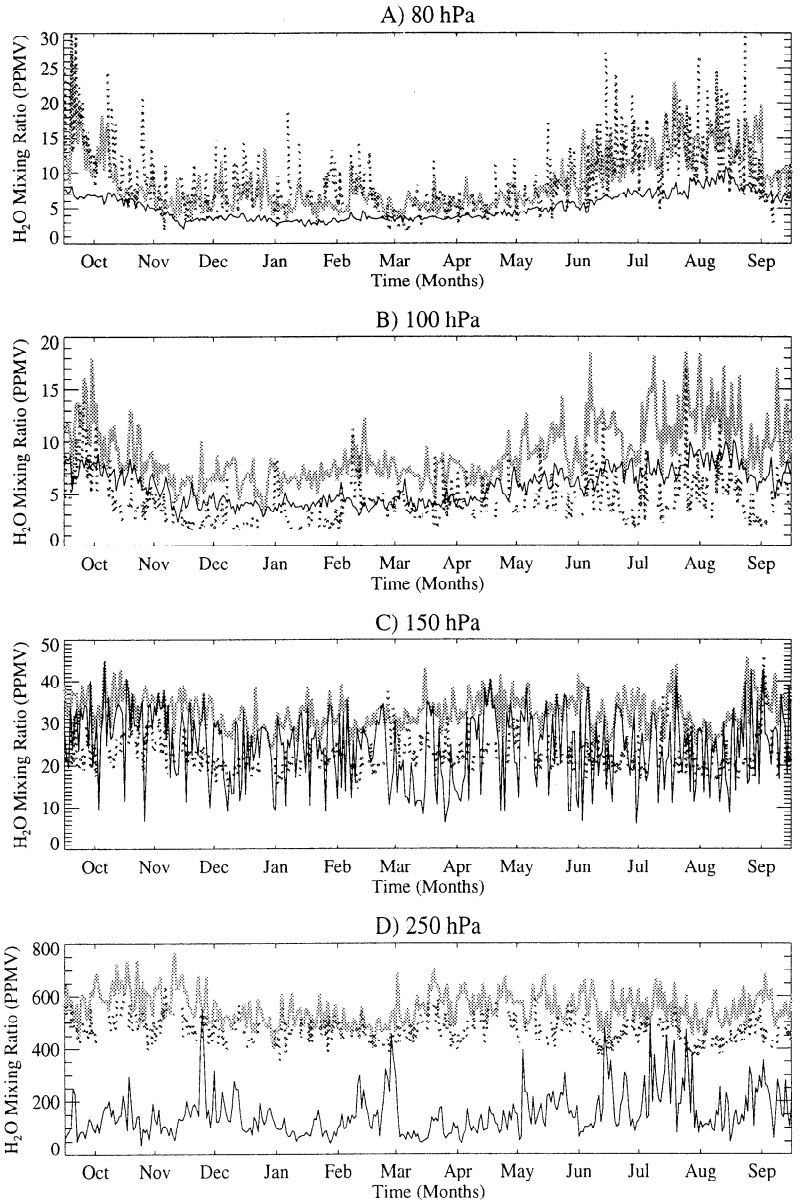

Figure 12. Simulated χ_{sat} (thick grey line), radiosonde χ_{sat} (black dotted line), and simulated tracer mixing ratio (thin solid line) at Koror (8°N, 135°E) in units of ppmv. Plots at different altitudes for 1 year of data. Model temperature and tracer data are interpolated to radiosonde mandatory reporting levels at (a) 80 hPa, (b) 100 hPa, (c) 150 hPa, and (d) 250 hPa.

hPa (Figure 12a) and 250 hPa (Figure 12d) simulated and observed χ_{sat} are quite similar. These results are similar for several stations examined in the Western Pacific, in the Indian Ocean, and in the tropical Atlantic. In the subtropical Central Pacific at Hilo (19°N and 165°W), the simulated and observed χ_{sat} are similar at 100 hPa and above the observed tracer concentration. Note that the tropopause at Hilo is above 100 hPa in the winter and below 100 hPa in the summer. In the simulation at Hilo, air is only near saturation (and above radiosonde saturation) at 150 hPa from July through October. Thus there are significant differences between the simulation and radiosonde observations of temperature only in the deep tropics (within 15° of the equator). The differences are consistent with the vertical distribution of assimilation temperature biases discussed in section 3 and consistent with higher than observed simulated tracer values in the upper tropical troposphere.

6. Stratosphere-Troposphere Exchange of Water Vapor

The simulated water vapor tracer, coupled with complete and consistent vertical velocity fields from the transport simulation, can also be used to examine details of the tropical cold point (the minimum in the vertical temperature profile) and the entry of water vapor into the stratosphere. The mass flux of water vapor

into the stratosphere can yield insights into whether the entry of air into the stratosphere is only through certain longitudinal regions (the "stratospheric fountain" hypothesis of *Newell and Gould-Stewart* [1981]) or whether water vapor is injected into the stratosphere at all longitudes [*Dessler*, 1998].

In the following discussion the tropics will be broken into four regions by longitude defined as follows: the "Indian" (IND) sector from the Greenwich meridian (0°) to 90°E, the "Western Pacific" (WPAC) sector from 90°E to the dateline (180°E), the "Eastern Pacific" (EPAC) from the dateline to 90°W, and the "Atlantic" (ATL) sector from 90°W to the Greenwich meridian. The Indian sector includes tropical African land regions, the Western Pacific includes the maritime continent, and the Atlantic sector includes tropical South America and part of Africa.

Fluxes of tracer across pressure surfaces were estimated by saving the pressure vertical velocity (ω—in mb day^{-1}) at each time step the tracer was saved. The vertical velocity is not an input meteorological variable. Rather, it is derived in the transport model from the convergence or divergence implied by the assimilated wind field. The vertical velocity contains significant variability on the smallest simulated time scales and space scales (1 day and hundreds of kilometers). Daily data are used, and no coherent trend or pattern is seen in the daily averages, so for presentation, results

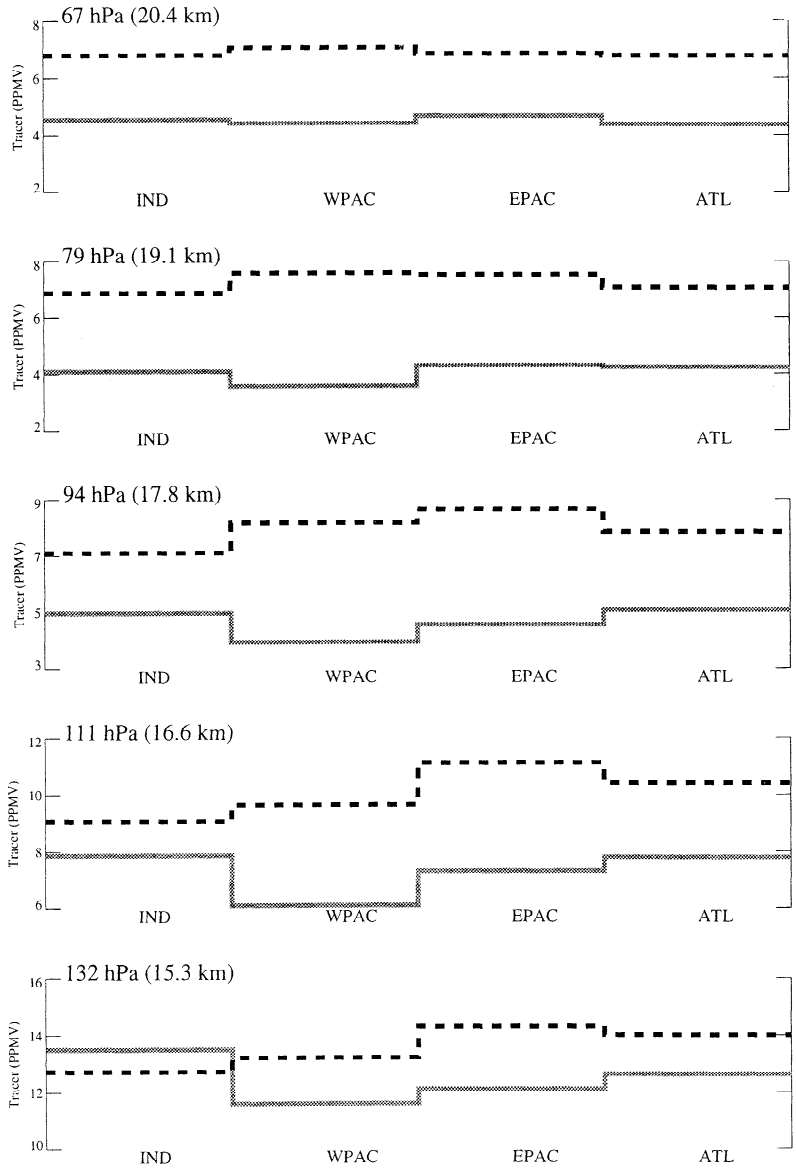

Figure 13. Tracer mixing ratio in units of ppmv averaged over tropical ($|\phi| < 15°$) sectors: Indian (IND), Western Pacific (WPAC), Eastern Pacific (EPAC), and Atlantic (ATL). Five different pressure levels are shown (log-pressure altitude in parentheses) for August (dotted lines) and February (solid lines).

are averaged over a month and a longitude sector of the deep tropics ($|\phi| < 15°$). The tracer flux ($-\omega\chi_t/g$) is a convolution of the tracer concentration with the air mass flux calculated at each grid point (so the zonal and eddy components are included). The average tracer concentrations for February and August are presented in Figure 13. There is zonal symmetry in tracer concentrations in the lower stratosphere (67 and 79 hPa) in both August and February. At 94 hPa and below (in the troposphere), average tracer concentrations vary significantly (by ~20%) between the different sectors. Tracer concentrations are significantly higher in August than February in the tropics. In February, tracer concentrations are lowest in the Western Pacific sector from 132 to 79 hPa, consistent with lower temperatures in this sector. Thus low mixing ratios are seen in the region of the tropical water vapor "fountain" at the cold point in the Western Pacific where temperatures are coldest in February. This result is consistent with the simulations of *Mote et al.* [1994].

The tracer fluxes by sector are illustrated in Figure 14 for model levels in the upper tropical troposphere and lower stratosphere. Note that the tropical upwelling region may extend poleward of 15° [*Rosenlof*, 1995; *Yang and Tung*, 1996], so only the deep tropics are captured in Figure 14. The tropical upward tracer flux is com-

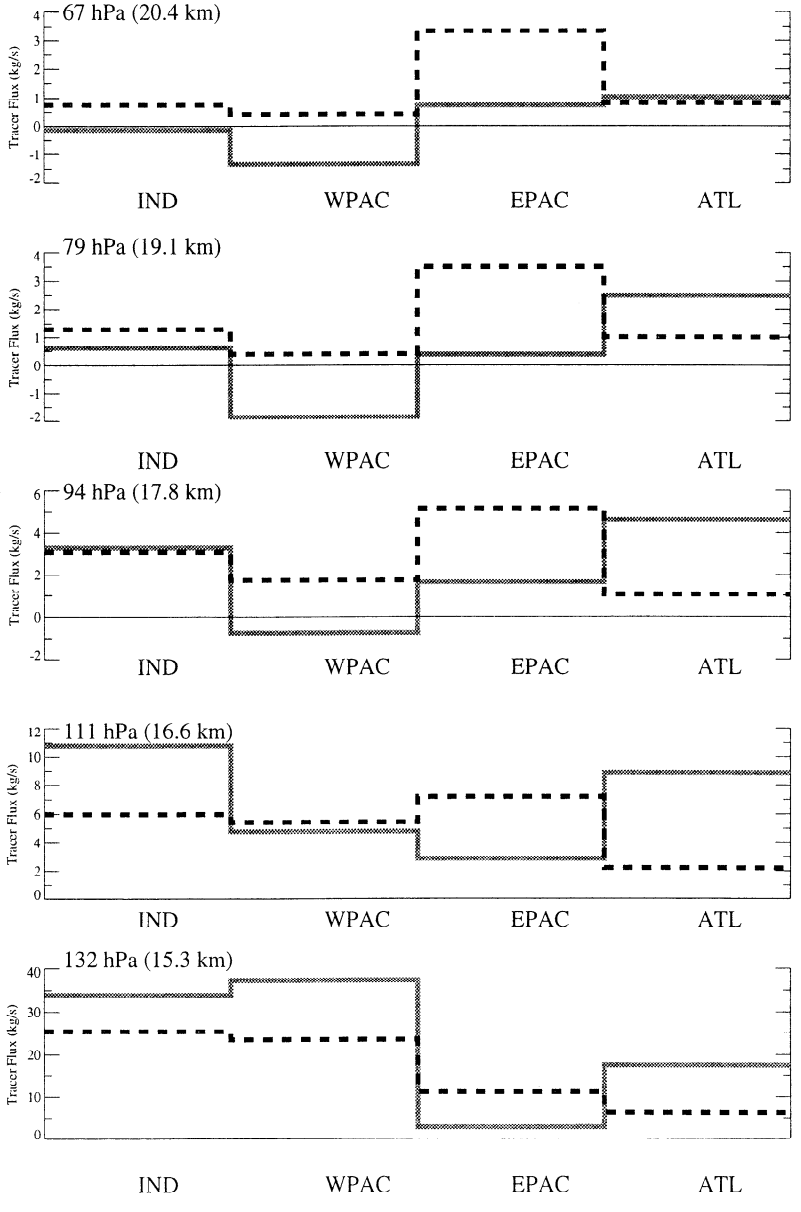

Figure 14. Average tracer mass flux (kg s^{-1}) averaged over tropical ($|\phi| < 15°$) sectors: Indian (IND), Western Pacific (WPAC), Eastern Pacific (EPAC), Atlantic (ATL). Five different pressure levels are shown (log-pressure altitude in parentheses) for August (dotted lines) and February (solid lines). Zero line is plotted as a thin solid line. Upward fluxes are positive.

parable between February and August. Air mass fluxes into the stratosphere are higher in February, consistent with the stratospheric circulation [*Rosenlof*, 1995], but tracer concentrations are higher in August (Figure 13). In the troposphere below 132 hPa (not shown), the tracer mass flux is largest in the Western Pacific sector in both February and August. The presence of the Asian monsoon circulation (a large upward flux in the Western Pacific) is notable up to 79 hPa in August if a broad region of the tropics and subtropics is analyzed ($|\phi| < 30°$).

At the cold point (79–94 hPa) and in the stratosphere (67 hPa), the largest upward tracer flux is over the Atlantic in February and over the Eastern Pacific in August. Over the Western Pacific in February at and above the cold point, the net water vapor fluxes are downward. This downward flux is consistent with the location of the stratospheric "drain" recently discussed by *Sherwood* [2000] in an analysis of radiosonde data. Using the radiosonde wind data over the Western Pacific, *Sherwood* [2000] calculated the vertical mass flux using the divergence of the winds from radiosondes along a closed contour. Above the cold point, a net downward motion was observed in the stratosphere. Such fluxes indicate that the assimilated wind and temperature fields at and above 100 hPa capture some of the effects of convective dehydration processes [*Sherwood*, 2000; *Danielsen*, 1993] that may significantly dehydrate the lower stratosphere. *Simmons et al.* [1999] also illustrate downward vertical velocities in ECMWF analyses over the Maritime Continent in the Western Pacific at 90 hPa in January. *Mote et al.* [1994] also indicate that in their simulations, the water vapor mass flux is downward at low water vapor mixing ratios, and the largest upward flux occurs at higher mixing ratios, broadly consistent with the results in this study.

A "fountain" (preferential regions or sectors where air enters the stratosphere) is not necessary, as noted by *Dessler* [1998], to explain the low water vapor mixing ratios in the stratosphere. Here we find generally higher averaged simulated tracer concentrations than observations of water vapor, but this is consistent with the temperature differences discussed in Section 3 and the mixing ratio on the entry of air into the stratosphere discussed in Section 5. The simulation is consistent with observations of subvisible cirrus clouds at longitudes outside of the Western Pacific [*Wang et al.*, 1996]. Such clouds are an indicator that rising motion is present at many longitudes in the tropics, which *Wang et al.* [1996] note is often correlated with convection.

The exchange of water vapor between the stratosphere and the troposphere does not occur simply across the tropical tropopause into the overworld. As discussed by *Holton et al.* [1995], there is significant quasi-isentropic exchange from the upper tropical troposphere into the extratropical lowermost stratosphere and vice versa. This exchange occurs when synoptic events create "tropopause folds" which significantly deform the tropopause structure [*Holton et al.*, 1995] and eventually result in "cut-off" cyclones and the deposition of stratospheric air into the troposphere and vice versa. *Postel and Hitchman* [1999] have characterized this exchange as Rossby wave breaking and analyzed the climatology of such events on the 350 K surface. The preferred locations for such events noted by *Postel and Hitchman* [1999] correspond to the planetary wave "ducts" of easterly winds in the tropics [*Webster*, 1983; *Webster and Holton*, 1982]. These events occur preferentially at different longitudes in each hemisphere (T. Horinouchi et al., Synoptic-scale Rossby waves and geographic distribution of lateral transport routes between the tropics and the extratropics in the lower stratosphere, submitted to *Journal of Geophysical Research*, 1999). Analysis of tracer maps on a pressure surface near 350 K (187 hPa) from the simulation yields a similar preferential distribution of high monthly average midlatitude tracer values in both hemispheres in winter. Analyzing daily tracer maps on a pressure surface from the simulation, these monthly averages are found to be the result of discrete "Rossby wave-breaking" events that transport air horizontally between the tropical troposphere and the extratropical lowermost stratosphere (and vice versa).

Another way of analyzing this exchange is by analyzing the transit time of water vapor from the tropical troposphere to high latitudes on a pressure or theta surface which spans the tropopause. In the stratospheric overworld (94 hPa), transit times are ~3–4 months (Figure 3), in agreement with HALOE observations at 380 K [*Rosenlof et al.*, 1997, Plate 6]. *Boering et al.* [1995] calculate a transit time in the lower part of the overworld from the tropics to midlatitudes of 4–6 months based on aircraft CO_2 and H_2O data. Using a model virtually identical to that in this work, *Strahan et al.* [1998] found rapid transport of the CO_2 signal from the tropics to midlatitudes in the lowermost stratosphere, and a delay of only 1–2 months exists between the arrival of the minimum concentration on 330 and 370 K at midlatitudes. *Strahan et al.* [1998] also found a difference in the annual cycle of CO_2 on either side of the midlatitude tropopause, consistent with analyses of in situ aircraft data. Fast transport from the surface to the middleworld (1.5 months) has also been recorded by *Ray et al.* [1999] in analyzing sulfur hexaflouride (SF_6) measurements on balloon flights. On the basis of the slope of simulated tracer isopleths in time at 220 hPa (~350 K) in the lowermost stratosphere (Figure 7), transit times from the tropics to midlatitudes are estimated to be 1–2 months, in agreement with the CO_2 simulations of *Strahan et al.* [1998] and the observations of *Ray et al.* [1999].

Unlike the CO_2 simulations of *Strahan et al.* [1998], we find no difference in the annual cycle of the water vapor tracer on either side of the tropopause. The annual signal in CO_2 is strongest in NH midlatitudes, where it must propagate to the tropics before entering the mid-

dleworld; hence a delay occurs between the midlatitude upper tropopause and lowermost stratosphere [*Strahan et al.*, 1998]. For water vapor, however, the annual cycle between the tropics and the extratropics is in phase (high in summer, low in winter), so no difference is noted on either side of the tropopause in the water vapor simulations conducted here.

7. Discussion and Conclusions

Assimilated winds and temperatures have been used with a global transport model to simulate the water vapor distribution. The parameterization includes only the effect of dehydration on water vapor. The variability of water vapor in the upper troposphere and lower stratosphere which emerges from these simulations is consistent with observations.

Quantitative estimates of the tracer mixing ratio in the stratospheric overworld are higher than observations (Table 1). The assimilated temperatures used have a known and defined warm bias at the tropical tropopause of 2–3 °K as described in Section 3. Given this bias, the higher water vapor concentrations in the simulation are expected, and no process other than the dehydration parameterized here is necessary to explain the net water vapor entry into the stratospheric overworld. The simulation implicitly includes convection, but the details of convection do not seem to be important for the water vapor burden in the stratosphere.

We also find that water vapor enters the stratospheric overworld (above the 380 K potential temperature surface) at all longitudes, not just in the western Pacific (Figure 14). While water vapor mixing ratios are lowest over the Western Pacific in February, at the cold point (94–79 hPa), net downward fluxes of water vapor are found. These downward fluxes are consistent with recent radiosonde analyses [*Sherwood*, 2000]. This conclusion is dependent upon the ability of the large-scale wind fields to correctly diagnose vertical motion. It is possible that the assimilation data may not give completely accurate results in the tropics. The most obvious failure of the assimilation data as utilized here is the lack of a convective contribution to the vertical motion field, which is likely important in the upper tropical troposphere as described below. The distribution of upwelling and downwelling regions in the tropics at 90–100 hPa in the simulated vertical velocity field is similar to the vertical velocity field in ECMWF analyses described by *Simmons et al.* [1999]. In particular, the ECMWF vertical velocity fields, and the simulations of *Mote et al.* [1994] (including convection) also found downward water vapor fluxes at 90-110 hPa over the maritime continent. While it is beyond the scope of this one year analysis, changes to the upper tropical tropospheric circulation resulting from the El-Nino–Southern Oscillation (ENSO) would be expected to modify the tropical Walker circulation, moving the region of convection eastward into the central and eastern Pacific [see *Webster and Chang*, 1988, Figure 1]. This might be expected to change the regions of upward and downward fluxes of water vapor at altitudes around the tropopause analyzed here, perhaps enhancing downward motions in the Western Pacific.

In between 80 and 200 hPa is a transition region where both local and nonlocal processes are important for determining the water vapor concentration and where the simulation does not capture the correct water vapor structure as inferred from radiosondes at 100 and 150 hPa (Figures 12b and 12c). These differences are too large to be explained by temperature biases alone. Convective processes are likely one of the reasons that the simulated tracer differs substantially from observations in the upper tropical troposphere between 200 and 100 hPa. It is likely that convection is very important in determining the smaller-scale vertical motion field. In addition, convective mechanisms for dehydration [*Danielsen*, 1982] and rehydration [*Vömel et al.*, 1995] are important for the water vapor distribution of the upper tropical troposphere. Wave driven modifications of the local temperature [*Fujiwara et al.*, 1998] or tropopause height [*Tsuda et al.*, 1994], as well as wave driven dehydration [*Potter and Holton*, 1995], may also be important in this transition region between the troposphere and the stratosphere. These processes may affect the lack of a "fountain" of air entering the stratosphere, and so this conclusion should be treated with some caution until it can be verified.

Several important conclusions can be drawn from the simulation about water vapor in the upper tropical troposphere and the exchange of water vapor across the tropopause. Large-scale advection alone is capable of producing much of the expected water vapor variability in the upper tropical troposphere. The conclusion is consistent with the work of *Salathé and Hartmann* [1997], *Pierrehumbert and Roca* [1998], and *Sherwood* [1996]. The upper tropical troposphere is tightly coupled by quasihorizontal exchange across the tropopause to the lowermost stratosphere in each hemisphere. Transport between the tropics and the extratropics in the middleworld and upper tropical troposphere appears to be well characterized by the simulation as described in section 6. Deficiencies in modeling the upper tropical troposphere between 200 hPa and the tropopause are likely the cause of high mixing ratios in the extratropical lowermost stratosphere not deficiencies in transport. Finally, the monsoon circulations figure prominently in the cycle of water vapor in the upper tropical troposphere and stratospheric middleworld. These circulations are important for moistening the extratropical lowermost stratosphere particularly in the Northern Hemisphere. Monsoon circulations also appear to moisten the lower stratospheric overworld.

This study suggests several avenues for further investigations to refine our understanding of the stratosphere-troposphere exchange of water vapor. Naturally, better assimilation data with more accurate tropopause tem-

peratures will be important for clarifying many of the issues raised in this study. Similar experiments in GCMs can help shed light on some of the processes not treated explicitly here but parameterized in GCMs (convection, gravity waves, and cloud microphysics). One important use might be the evaluation of different convective transport schemes. In addition, observations of the frequency of penetrating convection would help to quantify its potential role in stratosphere-troposphere exchange. Finally, better in situ observations of upper tropospheric temperature and water vapor would help refine some of the quantitative issues raised by this work and improve assimilation data sets.

Acknowledgments. We are grateful to C. W. Weaver and J. E. Nielsen for programming assistance and to two anonymous reviewers for their comments. AG was supported by a NASA Graduate Student Research Program Fellowship during the course of this work. Partial support at UW was provided by NASA Grant NAG-5-7090 (UARS). Computer resources were supported by the Atmospheric Chemistry Modeling and Analysis Program (ACMAP) at the Goddard Space Flight Center (A. Douglass, PI).

References

Appenzeller, C., J. R. Holton, and K. H. Rosenlof, Seasonal variation of mass transport across the tropopause, *J. Geophys. Res.*, *101*, 15,071–15,078, 1996.

Bjerknes, J., Atmospheric teleconnections from the equatorial pacific, *Mon. Weather Rev.*, *97*, 163–172, 1969.

Boering, K. A., et al., Measurements of stratospheric carbon dioxide and water vapor at northern midlatitudes: Implications for troposphere-to-stratosphere transport, *Geophys. Res. Lett.*, *22*, 2737–2740, 1995.

Brasseur, G. P., and S. Solomon, *Aeronomy of the Middle Atmosphere*, 2nd ed., D. Reidel, Norwell, Mass., 1986.

Brewer, A. W., Evidence for a world circulation provided by the measurements of helium and water vapor distribution in the stratosphere, *Q. J. R. Meteorol. Soc.*, *75*, 351–363, 1949.

Clark, H. L., R. S. Harwood, P. W. Mote, and W. G. Read, Variability of water vapor in the tropical upper troposphere as measured by the Microwave Limb Sounder on UARS, *J. Geophys. Res.*, *103*, 31,695–31,707, 1998.

Danielsen, E. F., A dehydration mechanism for the stratosphere, *Geophys. Res. Lett.*, *9*, 605–608, 1982.

Danielsen, E. F., In situ evidence of rapid, vertical, irreversible transport of lower tropospheric air into the lower tropical stratosphere by convective cloud turrets and by larger-scale upwelling in tropical cyclones, *J. Geophys. Res.*, *98*, 8665–8691, 1993.

Dessler, A. E., A reexamination of the "stratospheric fountain" hypothesis, *Geophys. Res. Lett.*, *25*, 4165–4168, 1998.

Douglass, A. R., C. J. Weaver, R. B. Rood, and L. Coy, A three-dimensional simulation of the ozone annual cycle using winds from a data assimilation system, *J. Geophys. Res.*, *101*, 1463–1474, 1996.

Fujiwara, M., K. Kita, and T. Ogawa, Stratosphere-troposphere exchange of ozone associated with the equatorial Kelvin wave as observed with ozonesondes and rawinsondes, *J. Geophys. Res.*, *103*, 19,173–19,182, 1998.

Gaffen, D. J., Radiosonde observations and their use in SPARC-related investigations, *SPARC Newsletter*, pp. 17–21, 1999.

Gill, A. E., *Atmosphere-Ocean Dynamics*, Academic, San Diego, Calif., 1982.

Hall, T. M., D. W. Waugh, K. A. Boering, and R. A. Plumb, Evaluation of transport in stratospheric models, *J. Geophys. Res.*, *104*, 18,815–18,839, 1999.

Hartmann, D. L., *Global Physical Climatology*, Int. Geophysics Ser., vol 56, Academic, San Diego, Calif., 1994.

Hintsa, E. J., et al., Troposphere to stratosphere transport in the lowermost stratosphere from measurements of H_2O, CO_2, N_2O and O_3, *Geophys. Res. Lett.*, *25*, 2655–2658, 1998.

Holton, J. R., P. H. Haynes, A. R. Douglass, R. B. Rood, and L. Pfister, Stratosphere–troposphere exchange, *Rev. Geophys.*, *33*, 403–439, 1995.

Hoskins, B. J., Towards a PV-θ view of the general circulation, *Tellus*, *43A-B*, 27–35, 1991.

Hurst, D. F., G. S. Dutton, P. A. Romashkin, P. R. Wamsley, F. L. Moore, J. W. Elkins, E. J. Hintsa, and E. M. Weinstock, Closure of the total hyrdogen budget of the Northern Hemisphere extratropical lower stratosphere, *J. Geophys. Res.*, *104*, 8191–8200, 1999.

Inamdar, A. K., and V. Ramanathan, Tropical and global scale interactions among water vapor, atmospheric greenhouse effect, and surface temperature, *J. Geophys. Res.*, *103*, 32,177–32,194, 1998.

Lin, S. J., and R. B. Rood, Multidimensional flux-form semilagrangian transport schemes, *Mon. Weather Rev.*, *124*, 2046–2070, 1996.

Madden, R. A., and P. R. Julian, Observations of the 40–50-day tropical oscillation—a review, *Mon. Weather Rev.*, *122*, 814–837, 1994.

Marti, J., and K. Mauersberger, A survey of new measurements of ice vapor pressure at temperatures between 170 and 250 K, *Geophys. Res. Lett.*, *20*, 363–366, 1993.

Mote, P. W., The annual cycle of stratospheric water vapor in a general circulation model, *J. Geophys. Res.*, *100*, 7363–7379, 1995.

Mote, P. W., J. R. Holton, and B. A. Boville, Characteristics of stratosphere-troposphere exchange in a general circulation model, *J. Geophys. Res.*, *99*, 16,815–16,829, 1994.

Mote, P. W., et al., An atmospheric tape recorder: The imprint of tropical tropopause temperatures on stratospheric water vapor, *J. Geophys. Res.*, *101*, 3989–4006, 1996.

Newell, R. E., and S. Gould-Stewart, A stratospheric fountain?, *J. Atmos. Sci.*, *38*, 2789–2796, 1981.

Newell, R. E., Y. Zhu, E. V. Browell, S. Ismail, W. G. Read, J. W. Waters, K. K. Kelly, and S. C. Liu, Upper tropospheric water vapor and cirrus: Comparison of DC-8 observations, preliminary UARS Microwave Limb Sounder measurements and meteorological analyses, *J. Geophys. Res.*, *101*, 1931–1941, 1996.

Pan, L., S. Solomon, W. Randel, J. F. Lamarque, P. Hess, J. Gille, E. W. Chiou, and M. P. McCormick, Hemispheric asymmetries and seasonal variations of the lowermost stratospheric water vapor and ozone derived from SAGE II data, *J. Geophys. Res.*, *102*, 28,177–28,184, 1997.

Pawson, S., and M. Fiorino, A comparison of reanalyses in the tropical stratosphere, Part 3, Inclusion of the pre-satellite data era, *Clim. Dyn.*, *15*, 241–250, 1999.

Pfister, L., K. R. Chan, T. P. Bui, S. Bowen, M. Legg, B. Gary, K. Kelly, M. Proffitt, and W. Starr, Gravity waves generated by a tropical cyclone during the STEP tropical field program: A case study, *J. Geophys. Res.*, *98*, 8611–8638, 1993.

Pierrehumbert, R. T., and R. Roca, Evidence for control of atlantic subtropical humidity by large scale advection, *Geophys. Res. Lett.*, *25*, 4537–4540, 1998.

Plumb, R. A., A "tropical pipe" model of stratospheric transport, *J. Geophys. Res.*, *101*, 3957–3972, 1996.

Postel, G. A., and M. H. Hitchman, A climatology of Rossby wave breaking along the subtropical tropopause, *J. Atmos. Sci.*, *56*, 359–373, 1999.

Potter, B. E., and J. R. Holton, The role of monsoon convection in the dehydration of the lower tropical stratosphere, *J. Atmos. Sci.*, *52*, 1034–1050, 1995.

Randel, W. J., F. Wu, J. M. Russell III, A. Roche, and J. W. Waters, Seasonal cycles and QBO variations in stratospheric CH_4 and H_2O observed in UARS HALOE data, *J. Atmos. Sci.*, *55*, 163–185, 1998.

Ray, E. A., et al., Transport into the northern hemisphere lowermost stratosphere revealed by in situ tracer measurements, *J. Geophys. Res.*, *104*, 26,565–26,580, 1999.

Read, W. G., J. W. Waters, D. A. Flower, L. Froidevaux, R. F. Jarnot, D. L. Hartmann, R. S. Harwood, and R. B. Rood, Upper tropospheric water vapor from UARS MLS, *Bull. Am. Meteorol. Soc.*, *76*, 2381–2389, 1995.

Reid, G. C., The tropical tropopause: Approaching a physical picture, *SPARC Newsletter*, *11*, 16–19, 1998.

Rosenfield, J. E., D. B. Considine, M. R. Schoeberl, and E. V. Browell, The impact of subvisible cirrus clouds near the tropopause on stratospheric water vapor, *Geophys. Res. Lett.*, *25*, 1883–1886, 1998.

Rosenlof, K. H., Seasonal cycle of the residual mean meridional circulation in the stratosphere, *J. Geophys. Res.*, *100*, 5173–5191, 1995.

Rosenlof, K., A. Tuck, K. Kelly, J. Russell III, and M. McCormick, Hemispheric asymmetries in water vapor and inferences about transport in the lower stratosphere, *J. Geophys. Res.*, *102*, 13,213–13,234, 1997.

Russell, J. M., et al., The halogen occultation experiment, *J. Geophys. Res.*, *98*, 10,777–10,797, 1993.

Salathé, E. P., and D. L. Hartmann, A trajectory analysis of tropical upper-tropospheric moisture and convection, *J. Atmos. Sci.*, *10*, 2533–2547, 1997.

Schoberl, M. R., C. H. Jackman, and J. Rosenfield, A Lagrangian estimate of aircraft effluent lifetime, *J. Geophys. Res.*, *103*, 10,817–10,825, 1998.

Schubert, S. D., R. B. Rood, and J. Pfaendtner, An assimilated dataset for earth science applications, *Bull. Am. Meteorol. Soc.*, *74*, 2331–2342, 1993.

Schubert, S. D., et al., A multi-year assimilation with the GEOS-1 system: Overview and results, *NASA Tech. Memo. 104606*, 1995.

Sherwood, S. C., Maintenance of the free-tropospheric tropical water vapor distribution, Part II, simulation by large scale advection, *J. Clim.*, *9*, 2919–2934, 1996.

Sherwood, S. C., A "stratospheric drain" over the maritime continent, *Geophys. Res. Lett.*, in press, 2000.

Simmons, A. J., A. Untch, C. Jakob, P. Kållberg, and P. Undén, Stratospheric water vapour and tropical tropopause temperatures in ECMWF analyses and multi-year simulations, *Q. J. R. Meteorol. Soc.*, *125*, 353–386, 1999.

Strahan, S. E., A. R. Douglass, J. E. Nielsen, and K. A. Boering, The CO_2 seasonal cycle as a tracer of transport, *J. Geophys. Res.*, *103*, 13,729–13,741, 1998.

Sun, D. Z., Distribution of tropical tropospheric water vapor, *J. Atmos. Sci.*, *50*, 1645–1660, 1993.

Tsuda, T., Y. Murayama, H. Wiryosumarto, S. W. B. Harijono, and S. Kato, Radiosonde observations of equatorial atmosphere dynamics over Indonesia: 1. equatorial waves and diurnal tides, *J. Geophys. Res.*, *99*, 10,491–10,505, 1994.

Vömel, H., S. Oltmans, D. Kley, and P. J. Crutzen, New evidence for the stratospheric dehydration mechanism in the equatorial pacific, *Geophys. Res. Lett.*, *22*, 3235–3238, 1995.

Wang, P. H., P. Minnis, M. P. McCormick, G. S. Kent, and K. M. Skeens, A 6-year climatology of cloud occurance frequency from Stratospheric Aerosol and Gas Experiment II observations (1985-1990), *J. Geophys. Res.*, *101*, 29,407–29,429, 1996.

Webster, P. J., Large-scale structure of the tropical atmosphere, in *Large-Scale Dynamical Processes in the Atmosphere*, edited by B. Hoskins and R. Pearce, pp. 235–275, Academic, San Diego, Calif., 1983.

Webster, P. J., and H. R. Chang, Equatorial energy accumulation and emanation regions: Impacts of a zonally varying basic state, *J. Atmos. Sci.*, *45*, 803–829, 1988.

Webster, P. J., and J. R. Holton, Cross equatorial response to middle-latitude forcing in a zonally varying basic state, *J. Atmos. Sci.*, *39*, 722–733, 1982.

Yang, H., and K. K. Tung, Cross-isentropic stratosphere-troposphere exchange of mass and water vapor, *J. Geophys. Res.*, *101*, 9413–9423, 1996.

Yulaeva, E., J. R. Holton, and J. M. Wallace, On the cause of the annual cycle in tropical lower-stratospheric temperatures, *J. Atmos. Sci.*, *51*, 169–174, 1994.

A. R. Douglass, Atmospheric Chemistry and Dynamics Branch, NASA Goddard Space Flight Center, Code 916 Greenbelt, MD 20771. (douglass@persephone.gsfc.nasa.gov)

A. Gettelman, Center for Atmospheric Research, Box 3000, Boulder, CO 80307. (andrew@ucar.edu)

J. R. Holton, Department of Atmospheric Sciences, University of Washington, Box 351640, Seattle, WA 98195-1640. (holton@atmos.washington.edu)

(Received June 30, 1999; revised November 12, 1999; accepted November 16, 1999.)